January 2009

# A field reconstruction technique for efficient modeling of the fields and forces within induction machines

Wu Dezheng

S. D. Pekarek

B. Fahimi



Dezheng, Wu; Pekarek, S. D.; and Fahimi, B., "A field reconstruction technique for efficient modeling of the fields and forces within induction machines" (2009). *Department of Electrical and Computer Engineering Faculty Publications.* Paper 30.
http://dx.doi.org/http://dx.doi.org/10.1109/TEC.2008.2001439

# A Field Reconstruction Technique for Efficient Modeling of the Fields and Forces Within Induction Machines

Dezheng Wu, Steven D. Pekarek, *Member, IEEE*, and Babak Fahimi, *Senior Member, IEEE*

***Abstract*—Traditional analysis and design of induction machines have been largely based upon lumped-parameter models. An alternative tool used for field-based evaluations of an induction machine is the finite-element method. Although useful, its computational complexity limits its use as a design tool. In this paper, a field reconstruction (FR) method for induction machine simulation is introduced. The FR method utilizes a small number of finite-element evaluations to establish basis functions of normal and tangential flux densities. The basis functions are then used to estimate the magnetic field under arbitrary stator excitation. Using such a tool, evaluation of fields and forces produced by a machine under alternative excitation strategies can be explored efficiently. Moreover, alternative field-based derivation of stator/rotor excitation control can be explored.**

***Index Terms*—Field reconstruction (FR), finite element (FE), induction machine, Maxwell stress tensor, torque and radial force.**

## I. Introduction

HISTORICALLY, the controls for induction-machine-based drives (i.e., field oriented [1]–[4], maximum torque/ampere [5]–[7], direct torque [8]–[12], volts/hertz, etc.) have been derived based upon the so-called lumped-parameter (LP) models of the machine. The LP models use inductance to relate winding current to the winding magnetic flux linkage. An energy-based approach is used to relate torque to the winding current and the partial derivatives (with respect to rotor position) of the stator–rotor mutual inductances. Although LP-based approaches have proven effective, they are based upon numerous assumptions, including that the stator and rotor windings are sinusoidally distributed, stator excitation is sinusoidal, harmonics due to stator and rotor slots are neglected, and that the magnetic field within the air gap is unidirectional (radial). In reality, the windings (particularly rotor windings) are rarely sinusoidally distributed, harmonics are present, and the forces acting within the machine are vectors (i.e., a normal and tangential component). The effects of different control strategies on the normal component of the forces, which is important for bearing wear, noise, etc., have been largely overlooked.

In this research, a fundamental question being raised is whether alternative excitation schemes for the induction machine can be developed using a field (rather than energy) based approach. In theory, the tools required to answer this question have been available for several years. Specifically, finite-element analysis (FEA) is well known as a tool for field-based analysis of electric machines. However, the computational effort required to complete a finite-element (FE) evaluation is significant even with modern processing power. This limits its usefulness as a tool for searching alternative excitation schemes. Therefore, as a first step, a new method for field-based evaluation of induction machines is proposed. In this so-called field reconstruction (FR) method, a small number of FE evaluations are used to determine the radial and tangential components of magnetic flux density within the air gap under single winding excitation. These results are then used to establish a basis set of magnetic flux densities, which are used to predict the fields and forces acting inside the machine under arbitrary stator excitation and rotor speed. Using the proposed approach, the computational effort to perform a field-based evaluation of the magnetic fields and forces can be reduced substantially. The proposed technique extends the FR method developed in [13], where the evaluation of the fields was within permanent magnet synchronous machines. The extension is nontrivial since the magnetic field produced by the rotor is induced rather than created by fixed magnet sources.

## II. Background

A three-phase, 60 Hz, four-pole, 5-hp squirrel-cage induction machine is studied as an example to demonstrate the process of FR. The machine topology is shown in Fig. 1. The induction machine contains 36 stator slots, 45 rotor slots, and 22 conductors per stator slot. The stator windings are wound at a full pitch. The dimensions of the machine are listed in Table I. Detailed dimensions of stator and rotor are also illustrated in Fig. 1. The dimension unit in the figure is millimeter.

In Fig. 1, the angular position along the stator circumference is denoted by $\phi_{\rm sm}$ and $\phi_{\rm rm}$ along the rotor circumference. The mechanical rotor position is denoted by $\theta_{\rm rm}$ and the mechanical angular velocity of the rotor is $\omega_{\rm rm}$. Based on the coordinate definitions, the following relationship is obtained:

$$\phi_{\rm sm} = \phi_{\rm rm} + \theta_{\rm rm}. \tag{1}$$

The calculation of forces used throughout the present paper is based upon the Maxwell stress tensor (MST) method. Using

Manuscript received September 20, 2007; revised February 20, 2008. Current version published May 19, 2009. This work was supported by the Electric Ship Research and Development Consortium (ESRDC) under Contract N00014-02-1-0623 with the Office of Naval Research. Paper no. TEC-00360-2007.

D. Wu and S. D. Pekarek are with the Department of Electrical and Computer Engineering, Purdue University, West Lafayette, IN 47907 USA (e-mail: wu54@purdue.edu; spekarek@purdue.edu).

B. Fahimi is with the Department of Electrical Engineering, University of Texas at Arlington, Arlington, TX 76019 USA (e-mail: fahimi@uta.edu).

Color versions of one or more of the figures in this paper are available online at http://ieeexplore.ieee.org.

Digital Object Identifier 10.1109/TEC.2008.2001439

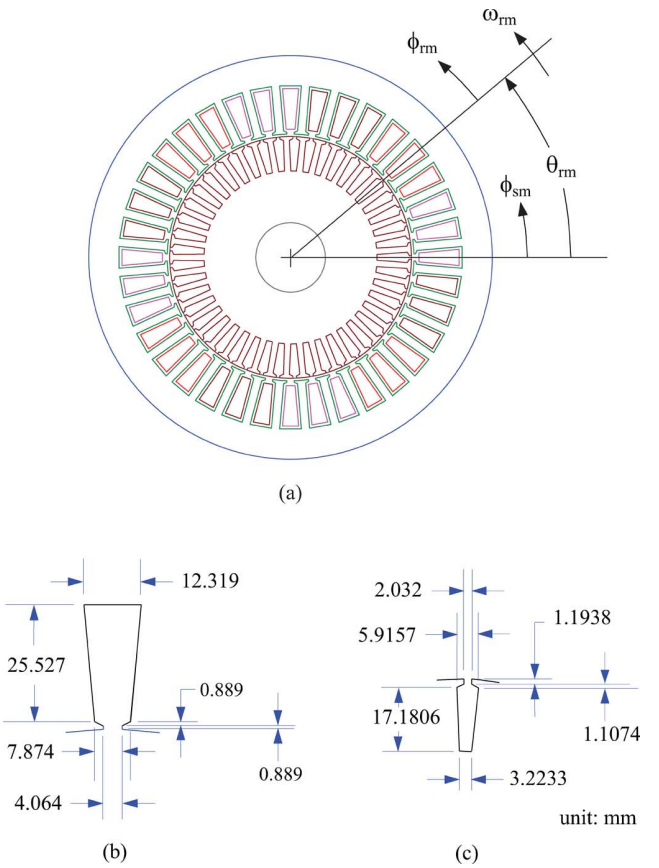


Fig. 1. Three-phase four-pole squirrel-cage induction machine. (a) Cross-section view of the induction machine and coordinate system. (b) Stator slot dimension. (c) Rotor slot dimension.

TABLE I
INDUCTION MACHINE PARAMETERS

| Machine parameters | Value |
|---|---|
| Rated voltage | 208 V rms L-L |
| Rated speed | 1760 rpm |
| Rated torque | 20.23 Nm |
| Airgap | 1.42 mm |
| Rotor outer diameter | 136.92 mm |
| Stator outer diameter | 228.6 mm |
| Stack length | 88.9 mm |
| Shaft diameter | 39.4 mm |
| Lamination material | M-19 |
| Stator winding material | Copper |
| Rotor bar material | Aluminum |
| Number of turns per coil | 22 |
| Number of coils per phase | 6 coils in series connection |

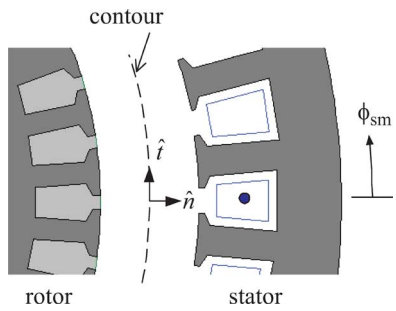


Fig. 2. Normal and tangential direction.

the MST method, the amplitude of the tangential and normal force densities in the air gap can be expressed as [14]

$$f_t = \frac{B_n B_t}{\mu_0} \tag{2}$$

$$f_n = \frac{\left(B_n^2 - B_t^2\right)}{2\mu_0} \tag{3}$$

where $B_n$ and $B_t$ are normal and tangential components of the magnetic flux density, respectively, and $\mu_0$ is the permeability of air. The positive current, normal, and tangential directions are defined in Fig. 2.

Therefore, the electromagnetic torque is obtained by

$$T_e = F_t R\, l_z = \frac{R\, l_z}{\mu_0} \oint_{\Gamma} B_n B_t\, \hat{t} \cdot d\vec{l} \tag{4}$$

where $R$ is the radius of the integration contour, $\hat{t}$ is the unit vector of tangential direction, and $l_z$ is the effective stack length. The contour $\Gamma$ is the circular integration contour in the air gap. In this paper, the contour is established in the middle of the air gap to minimize numerical error of the MST method [15]. Here, a similar integral is defined to represent radial force over an electric cycle. Specifically,

$$F_n = \int_0^{2\pi} f_n R\, d\phi_s = \frac{R}{2\mu_0} \int_0^{2\pi} \left(B_n^2 - B_t^2\right) d\phi_s \tag{5}$$

where $\phi_s = \phi_{\rm sm} P/2$ is the so-called electric angle and $P$ is the number of poles. The radial force defined in (5) is the integration of stress. In practice, $B_n$ is greater than $B_t$, and therefore, this stress is always positive, which means the radial force density is in the normal direction from rotor to stator over the contour. The nonzero value of $F_n$ in (5) does not mean that there is a net force acting to push/pull the stator and rotor. Actually, the net radial force acting on the rotor is zero for a balanced excitation and uniform machine structure.

The following assumptions have been made for the analysis in this paper. The stator teeth and rotor teeth are assumed to be rigid, i.e., no deformation due to radial and tangential force occurs in these parts. The flux density in the axial direction is zero, which means no end effect exists. Hysteresis and eddy currents in the stator and rotor iron are neglected. The operating temperature is assumed to be constant (or the effect of temperature variation to machine parameters is neglected).

## III. FIELD CHARACTERIZATION

To develop the FR method for an induction machine, it is assumed that the machine operates in the linear magnetic region (which is consistent with assumptions used in the derivation of many LP models). Under the assumption of linearity, the superposition rule can be applied. Therefore, the FR begins by considering the normal and tangential components of flux

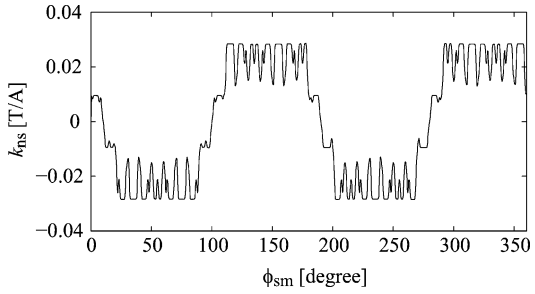


Fig. 3. Basis function $k_{\rm ns}(\phi_{\rm sm})$.

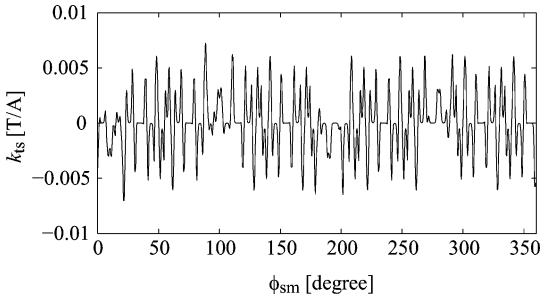


Fig. 4. Basis function $k_{\rm ts}(\phi_{\rm sm})$.

density in terms of stator and rotor quantities, i.e.,

$$B_n(\phi_{\rm sm}) = B_{\rm ns}(\phi_{\rm sm}) + B_{\rm nr}(\phi_{\rm sm}, \theta_{\rm rm}) \tag{6}$$

$$B_t(\phi_{\rm sm}) = B_{\rm ts}(\phi_{\rm sm}) + B_{\rm tr}(\phi_{\rm sm}, \theta_{\rm rm}). \tag{7}$$

In (6) and (7), $B_{\rm ns}$ and $B_{\rm ts}$ are normal and tangential components of the flux density directly generated by stator current. $B_{\rm nr}$ and $B_{\rm tr}$ are normal and tangential components of the flux density generated by rotor currents. The current in the rotor bars is induced by the variations of the magnetic field, which results from stator current excitation and rotor motion. The basis of the FR method is to create models for each of the components in (6) and (7) using only a few FEA evaluations. This is achieved by a two-step procedure consisting of "stator" and "rotor" basis function derivation.

### A. Stator Basis Function Derivation

As the first step, a magnetostatic FEA program (which is relatively time-efficient) is used to derive the stator basis function. In the FEA program, the rotor is fixed at an arbitrary position and the phase current is set such that $i_{\rm as} = 1$ A with phase-*b* and phase-*c* open. The normal and tangential components of the flux density in the air gap are calculated and stored as the basis functions $k_{\rm ns}(\phi_{\rm sm})$ and $k_{\rm ts}(\phi_{\rm sm})$, respectively. In order to store the basis functions, the air gap contour $\Gamma$ is discretized into *n* equally distributed points. Hence, $k_{\rm ns}(\phi_{\rm sm})$ and $k_{\rm ts}(\phi_{\rm sm})$ are represented as two $n \times 1$ vectors in the computer. The stator basis functions for the given machine are shown in Figs. 3 and 4, respectively.

Using these basis functions, the flux density generated by arbitrary stator phase-*a* current can be expressed as

$$B_{\rm nas}(\phi_{\rm sm}) = i_{\rm as} k_{\rm ns}(\phi_{\rm sm}) \tag{8}$$

$$B_{\rm tas}(\phi_{\rm sm}) = i_{\rm as} k_{\rm ts}(\phi_{\rm sm}). \tag{9}$$

Due to symmetry, the flux densities generated by phase-*b* and phase-*c* current are obtained using a phase shift of the respective basis functions. Thus, the total normal and tangential components of the flux density directly generated by the stator current are obtained by

$$B_{\rm ns}(\phi_{\rm sm}) = i_{\rm as} k_{\rm ns}(\phi_{\rm sm}) + i_{\rm bs} k_{\rm ns}\left(\phi_{\rm sm} - \frac{2}{P}\frac{2\pi}{3}\right) + i_{\rm cs} k_{\rm ns}\left(\phi_{\rm sm} - \frac{2}{P}\frac{4\pi}{3}\right) \tag{10}$$

$$B_{\rm ts}(\phi_{\rm sm}) = i_{\rm as} k_{\rm ts}(\phi_{\rm sm}) + i_{\rm bs} k_{\rm ts}\left(\phi_{\rm sm} - \frac{2}{P}\frac{2\pi}{3}\right) + i_{\rm cs} k_{\rm ts}\left(\phi_{\rm sm} - \frac{2}{P}\frac{4\pi}{3}\right). \tag{11}$$

### B. Rotor Basis Function Derivation

Unlike $B_{\rm ns}$ and $B_{\rm ts}$, the flux density components generated by rotor currents are not only determined by the instantaneous stator current, but they are also determined due to the change in the stator current. In other words, $B_{\rm nr}$ and $B_{\rm tr}$ are the flux densities generated by the rotor current, which results from the stator current and rotor motion. To identify and store rotor basis functions, the air gap contour $\Gamma$ is discretized into *n* equally distributed points as in the stator basis function derivation. The rotor basis functions ($k_{\rm nr}$ and $k_{\rm tr}$), which represent the relationship between $B_{\rm nr}$, $B_{\rm tr}$, and the stator current, are characterized in time domain. To identify the rotor basis functions, the rotor speed is set at $\omega_{\rm rm} = 0$. Using a transient FEA solver, a discrete impulse is used as the phase-a current input signal. The impulse input signal has a value of $I_0$ at $t_j$ and 0 elsewhere, i.e.,

$$i_{\rm as}(t_k) = \begin{cases} I_0, & k = j \\ 0, & k \neq j. \end{cases} \tag{12}$$

In this research, the software Ansoft Maxwell 2-D is used for FEA computation. The impulse current signal is defined in Maxwell 2-D. When setting the impulse input, an "IF" command that defines $I_0$ at a time step and 0 elsewhere is used. The command in the Maxwell 2-D is "if(T = 0.001,20,0)." The characterization of rotor basis function requires the FEA model to run over a period of time in order to capture sufficient data for subsequent studies. During the calculation time, all the normal and tangential components of the air gap flux density at $t \geq t_j$ are recorded as $B_{\rm nid}(\tau)$ and $B_{\rm tid}(\tau)$, where $\tau = t - t_j$. Since the derivation of the rotor basis functions is the eventual desired knowledge, the flux directly contributed by the stator current ($i_{\rm as}k_{\rm ns}$ and $i_{\rm as}k_{\rm ts}$) is subtracted. Specifically, using the previously established stator basis functions, the normal and tangential components of the flux density generated by the rotor currents $B_{\rm nr}$ and $B_{\rm tr}$ are represented by

$$B_{\rm nr} = B_{\rm nid} - i_{\rm as} k_{\rm ns} \tag{13}$$

$$B_{\rm tr} = B_{\rm tid} - i_{\rm as} k_{\rm ts}. \tag{14}$$

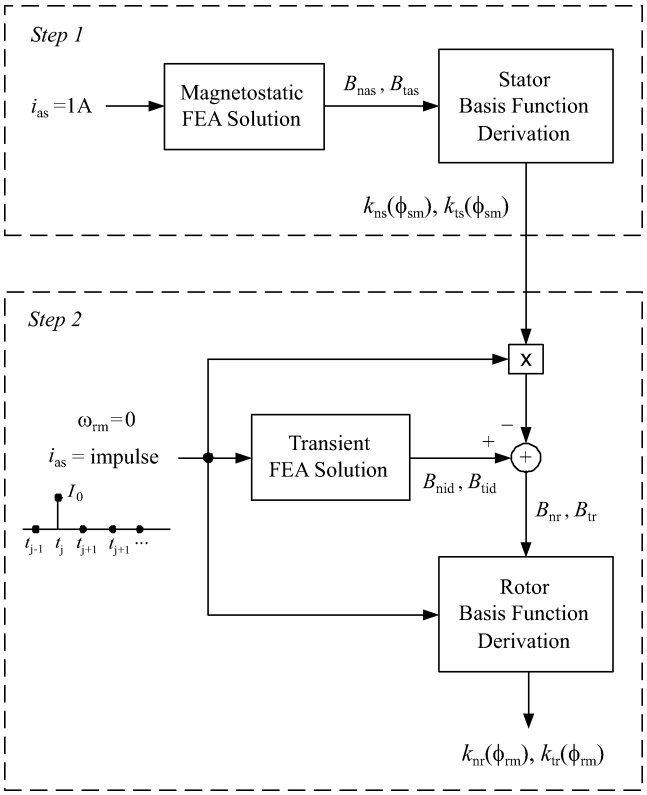


Fig. 5. Two-step procedure of basis function identification.

$B_{\rm nr}$ and $B_{\rm tr}$ are then divided by $I_0$ to get the unit rotor impulse response $k_{\rm nr}$ and $k_{\rm tr}$ as

$$k_{\rm nr} = \frac{B_{\rm nr}}{I_0} \tag{15}$$

$$k_{\rm tr} = \frac{B_{\rm tr}}{I_0}. \tag{16}$$

The unit impulse response is then defined as the rotor basis functions and stored in the computer. Using this approach, the rotor basis functions $k_{\rm nr}$ and $k_{\rm tr}$ are expressed as two matrices. The rows of the matrices represent the *n* points along the contour, and the columns of the matrices describe the impulse response of these points in the discrete-time domain. The two-step procedure for identification of the basis functions based upon phase-*a* stator excitation is shown in Fig. 5.

The rotor model is assumed to be linear, so the output is regarded as the sum of responses to a sequence of discrete-time impulse input. This is evaluated using convolution in the time domain. The obtained rotor basis function can also be used in phase-*b* and phase-*c* by using a phase shift similar as in (10) and (11). Therefore, with arbitrary stator current, the flux density generated by the rotor is obtained from the rotor basis functions

$$\begin{aligned} B_{\rm nr}\left(\phi_{\rm rm}, t\right) &= i_{\rm as}\left(t\right) * k_{\rm nr}\left(\phi_{\rm rm}, t\right) \\ &+ i_{\rm bs}\left(t\right) * k_{\rm nr}\left(\phi_{\rm rm} - \frac{2}{P}\frac{2\pi}{3}, t\right) \\ &+ i_{\rm cs}\left(t\right) * k_{\rm nr}\left(\phi_{\rm rm} - \frac{2}{P}\frac{4\pi}{3}, t\right) \end{aligned} \tag{17}$$

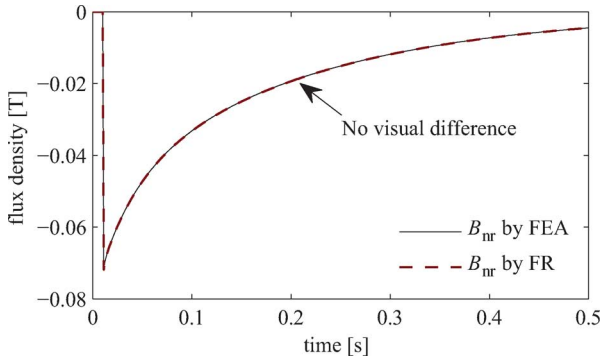


Fig. 6. Step response of rotor basis function $k_{\rm nr}(\phi_{\rm sm} = 0)$ produced by the FEA program and the FR rotor basis function.

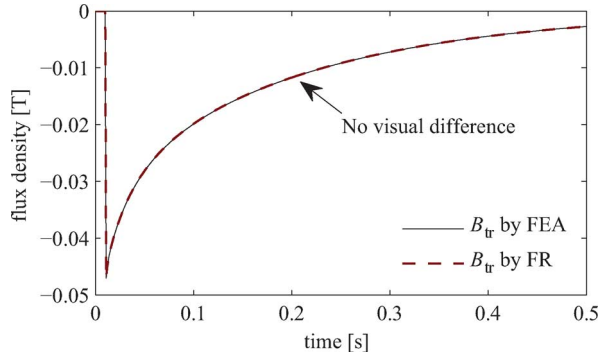


Fig. 7. Step response of rotor basis function $k_{\rm tr}(\phi_{\rm sm} = 0)$ produced by the FEA program and the FR rotor basis function.

$$\begin{aligned} B_{\rm tr}\left(\phi_{\rm rm}, t\right) &= i_{\rm as}\left(t\right) * k_{\rm tr}\left(\phi_{\rm rm}, t\right) \\ &+ i_{\rm bs}\left(t\right) * k_{\rm tr}\left(\phi_{\rm rm} - \frac{2}{P}\frac{2\pi}{3}, t\right) \\ &+ i_{\rm cs}\left(t\right) * k_{\rm tr}\left(\phi_{\rm rm} - \frac{2}{P}\frac{4\pi}{3}, t\right) \end{aligned} \tag{18}$$

where "$*$" denotes the operation of convolution.

To verify the accuracy of the rotor basis functions, the step responses of $B_{\rm nr}$ and $B_{\rm tr}$ are obtained using the FEA program and the FR method. For simplicity, it is assumed that phase-*b* and phase-*c* stator current are kept zero. The rotor speed is also assumed to be zero. At $t = 0.01$ s, the phase-*a* current $i_{\rm as}$ has a step change from 0 to 10 A, and it is set to be 10 A thereafter. The flux density contributed by the rotor current at position $\phi_{\rm sm} = 0$ is selected to be investigated. Fig. 6 shows the step responses of $B_{\rm nr}(\phi_{\rm sm} = 0)$ versus time, while the step responses of $B_{\rm tr}(\phi_{\rm sm} = 0)$ versus time are compared in Fig. 7. It is observed that the outputs of FR rotor basis function are visually indistinguishable from FEA program results.

## IV. Field Reconstruction

Having stator and rotor basis functions, the overall flux densities are obtained by (6) and (7) with arbitrary stator current

excitation and motor speed. Radial and tangential forces are also determined from the reconstruction result of the air gap flux density. In (17) and (18), $B_{\rm nr}$ and $B_{\rm tr}$ are obtained in terms of the rotor coordinate $\phi_{\rm rm}$. Therefore, in order to evaluate the overall flux density in terms of stator coordinate $\phi_{\rm sm}$, a substitution is applied to $B_{\rm nr}$ and $B_{\rm tr}$ using $\phi_{\rm rm} = \phi_{\rm sm} - \theta_{\rm rm}$. Then, by substituting (10) and (11) and (17) and (18) into (6) and (7), we have

$$\begin{aligned} B_n(\phi_{\rm sm}, t) &= i_{\rm as}(t)\, k_{\rm ns}(\phi_{\rm sm}) + i_{\rm as}(t) * k_{\rm nr}(\phi_{\rm sm} - \theta_{\rm rm}, t) \\ &\quad + i_{\rm bs}(t)\, k_{\rm ns}\left(\phi_{\rm sm} - \frac{2}{P}\frac{2\pi}{3}\right) \\ &\quad + i_{\rm bs}(t) * k_{\rm nr}\left(\phi_{\rm sm} - \theta_{\rm rm} - \frac{2}{P}\frac{2\pi}{3}, t\right) \\ &\quad + i_{\rm cs}(t)\, k_{\rm ns}\left(\phi_{\rm sm} - \frac{2}{P}\frac{4\pi}{3}\right) \\ &\quad + i_{\rm cs}(t) * k_{\rm nr}\left(\phi_{\rm sm} - \theta_{\rm rm} - \frac{2}{P}\frac{4\pi}{3}, t\right) \end{aligned} \tag{19}$$

$$\begin{aligned} B_t(\phi_{\rm sm}, t) &= i_{\rm as}(t)\, k_{\rm ts}(\phi_{\rm sm}) + i_{\rm as}(t) * k_{\rm tr}(\phi_{\rm sm} - \theta_{\rm rm}, t) \\ &\quad + i_{\rm bs}(t)\, k_{\rm ts}\left(\phi_{\rm sm} - \frac{2}{P}\frac{2\pi}{3}\right) \\ &\quad + i_{\rm bs}(t) * k_{\rm tr}\left(\phi_{\rm sm} - \theta_{\rm rm} - \frac{2}{P}\frac{2\pi}{3}, t\right) \\ &\quad + i_{\rm cs}(t)\, k_{\rm ts}\left(\phi_{\rm sm} - \frac{2}{P}\frac{4\pi}{3}\right) \\ &\quad + i_{\rm cs}(t) * k_{\rm tr}\left(\phi_{\rm sm} - \theta_{\rm rm} - \frac{2}{P}\frac{4\pi}{3}, t\right). \end{aligned} \tag{20}$$

Care must be exercised in evaluating (19) and (20) as it can be seen that $\theta_{\rm rm}$ changes with time when $\omega_{\rm rm} \neq 0$. The physical meaning of the substitution $\phi_{\rm rm} = \phi_{\rm sm} - \theta_{\rm rm}$ is to include the rotation of the rotor magnet field. Since the rotor flux is generated by the rotor current in cage bars, it also rotates with the rotor. Since the rotor basis functions $k_{\rm nr}$ and $k_{\rm tr}$ are characterized in the discrete-time form, it is more convenient to evaluate the convolution in (19) and (20) in discrete-time domain. It is important to remember that we are assuming that the relationship between the stator current and rotor magnetic system is linear. In addition, for the studies conducted herein, it is also assumed that the rotor basis functions are independent of rotor position. Using rotor basis functions that are position dependent is discussed in Section VI.

As a reminder, the output of any discrete-time linear system can be expressed in terms of the input as

$$y(k) = u(k) * h(k) \tag{21}$$

where $u(k)$ is the input and $h(k)$ is the discrete-time impulse response [16]. The discrete-time impulse response can be obtained by providing a discrete-time delta function as the system input. The resulting calculated output is the impulse response [16]. Note that the convolution of two signals $u(k)$ and $h(k)$ is defined as [16]

$$u(k) * h(k) = \sum_{m=1}^{k} u(m) h(k-m). \tag{22}$$

In the proposed modeling approach, the rotor basis functions $k_{\rm nr}$ and $k_{\rm tr}$ are expressed as unit impulse responses. As a result, the rotor flux density is equal to the convolution of stator current and the rotor basis function, and (19) and (20) are expressed as

$$\begin{aligned} &B_n(\phi_{\rm sm}, t_k) \\ &= i_{\rm as}(t_k)\, k_{\rm ns}(\phi_{\rm sm}) + i_{\rm bs}(t_k)\, k_{\rm ns}\left(\phi_{\rm sm} - \frac{2}{P}\frac{2\pi}{3}\right) \\ &\quad + i_{\rm cs}(t_k)\, k_{\rm ns}\left(\phi_{\rm sm} - \frac{2}{P}\frac{4\pi}{3}\right) \\ &\quad + \sum_{m=1}^{k} i_{\rm as}(t_m)\, k_{\rm nr}(\phi_{\rm sm} - \theta_{\rm rm}(t_k) + \theta_{\rm rm}(t_m), t_k - t_m) \\ &\quad + \sum_{m=1}^{k} i_{\rm bs}(t_m)\, k_{\rm nr}\left(\phi_{\rm sm} - \theta_{\rm rm}(t_k) + \theta_{\rm rm}(t_m) - \frac{2}{P}\frac{2\pi}{3}, t_k - t_m\right) \\ &\quad + \sum_{m=1}^{k} i_{\rm cs}(t_m)\, k_{\rm nr}\left(\phi_{\rm sm} - \theta_{\rm rm}(t_k) + \theta_{\rm rm}(t_m) - \frac{2}{P}\frac{4\pi}{3}, t_k - t_m\right) \end{aligned} \tag{23}$$

$$\begin{aligned} &B_t(\phi_{\rm sm}, t_k) \\ &= i_{\rm as}(t_k)\, k_{\rm ts}(\phi_{\rm sm}) + i_{\rm bs}(t_k)\, k_{\rm ts}\left(\phi_{\rm sm} - \frac{2}{P}\frac{2\pi}{3}\right) \\ &\quad + i_{\rm cs}(t_k)\, k_{\rm ts}\left(\phi_{\rm sm} - \frac{2}{P}\frac{4\pi}{3}\right) \\ &\quad + \sum_{m=1}^{k} i_{\rm as}(t_m)\, k_{\rm tr}(\phi_{\rm sm} - \theta_{\rm rm}(t_k) + \theta_{\rm rm}(t_m), t_k - t_m) \\ &\quad + \sum_{m=1}^{k} i_{\rm bs}(t_m)\, k_{\rm tr}\left(\phi_{\rm sm} - \theta_{\rm rm}(t_k) + \theta_{\rm rm}(t_m) - \frac{2}{P}\frac{2\pi}{3}, t_k - t_m\right) \\ &\quad + \sum_{m=1}^{k} i_{\rm cs}(t_m)\, k_{\rm tr}\left(\phi_{\rm sm} - \theta_{\rm rm}(t_k) + \theta_{\rm rm}(t_m) - \frac{2}{P}\frac{4\pi}{3}, t_k - t_m\right). \end{aligned} \tag{24}$$

As an example to illustrate how this is performed, it is convenient to assume that the stator current $i_{\rm as} = 10\cos(377t)$, $i_{\rm bs} = 0$, $i_{\rm cs} = 0$, and the rotor speed $\omega_{\rm rm} = 17.45$ rad/s $= 1000^\circ/$s. The step size is 0.001 s, which means that the rotor angle $\theta_{\rm rm}$ has

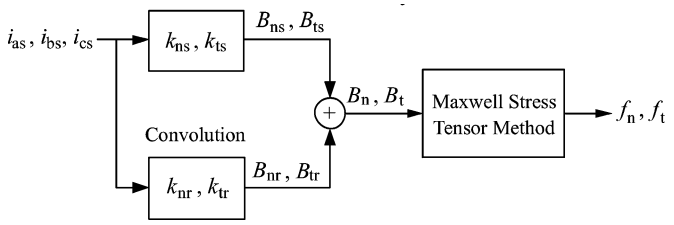


Fig. 8. FR process.

an incremental of 1°/step. $B_n$ at $\phi_{\rm sm} = 60°$, time $t_k$ is calculated using (23) as

$$\begin{aligned} &B_n\left(60^\circ, t_k\right) \\ &\quad = k_{\rm ns}\left(60^\circ\right) i_{\rm as}\left(t_k\right) + k_{\rm nr}\left(60^0, 0\,{\rm s}\right) i_{\rm as}\left(t_k\right) \\ &\qquad + k_{\rm nr}\left(59^\circ, 0.001\,{\rm s}\right) i_{\rm as}\left(t_k - 0.001\,{\rm s}\right) \\ &\qquad + k_{\rm nr}\left(58^\circ, 0.002\,{\rm s}\right) i_{\rm as}\left(t_k - 0.002\,{\rm s}\right) + \cdots . \end{aligned} \quad (25)$$

In (25), the second term on the right-hand side is the rotor flux due to $i_{\rm as}(t_k)$, and the third term is rotor flux due to the input at previous step $i_{\rm as}(t_k - 0.001\ {\rm s})$.

The reconstruction process is illustrated in Fig. 8, wherein based upon the respective stator phase current inputs, the FR model calculates normal and tangential components of the magnetic flux and force densities under arbitrary stator excitation.

## V. Results

To validate the effectiveness of the proposed FR technique, two common induction motor drive cases are simulated. In order to derive machine basis functions and compare simulation results, Ansoft Maxwell is used to implement an FEA-based model of the induction machine [17]. The FR program was implemented in MATLAB. A 3.19 GHz P4 PC is used to perform the FEA and the FR programs. In selecting the step size, one is effectively adjusting the sampling frequency, and therefore, adjusting the bandwidth over which the FR model will match. The choice of the step size depends accordingly upon the dynamic of the respective input waveform. In this paper, the input current has the frequency up to 60 Hz; therefore, the step size of 1 ms is taken.

### A. Constant-Speed Operation

Simulation of constant-speed operation is helpful to evaluate the steady-state performance of the induction motor drive. In this case, it is assumed that the motor is operated at a constant speed of 1333.3 r/min. At $t = 0$ s, the commanded three-phase currents has a step change from 0 to $i_{\rm as} = 20\sin(100\pi t)$, $i_{\rm bs} = 20\sin(100\pi t - 2\pi/3)$, $i_{\rm cs} = 20\sin(100\pi t + 2\pi/3)$. The step sizes for both methods are 0.001 s. To characterize the machine behavior, it requires an FEA program 220 min to simulate the induction machine dynamics from 0 to 1.5 s, while the FR method needs 40 s. The flux density results generated by FEA and FR programs at $t = 0.255$ s are compared in the Figs. 9 and 10. The normal component of the flux density in the air gap is shown in Fig. 9. The tangential component of flux densities is shown in Fig. 10. It is observed that FEA and FR techniques produce almost identical flux density results in the air gap.

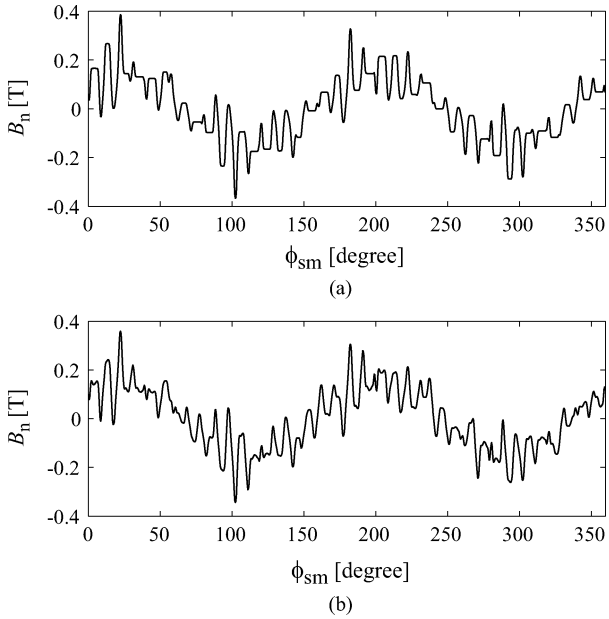


Fig. 9. Normal component of the flux density in the air gap. (a) FEA result. (b) FR result.

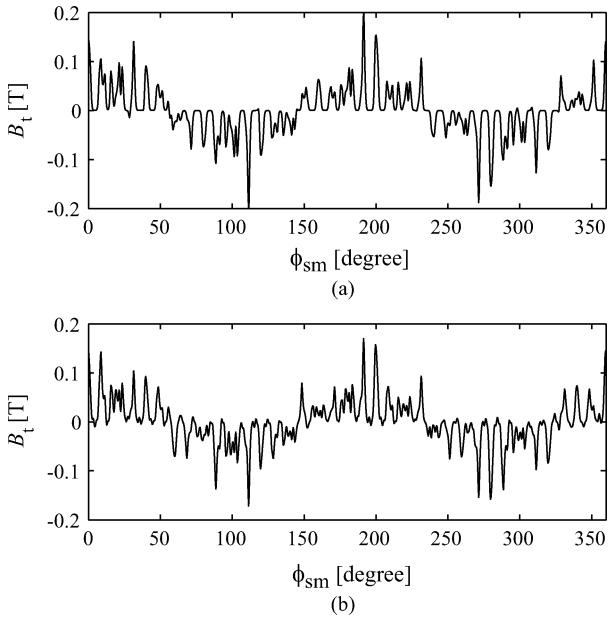


Fig. 10. Tangential component of the flux density in the air gap. (a) FEA result. (b) FR result

In Fig. 11, the electromagnetic torque predicted by FEA and FR programs is compared. The calculated radial forces using these two methods are also shown. In the figure, the solid lines are for the FEA result and the dashed lines are for the FR result. The proposed FR method demonstrates satisfactory accuracy at only a small fraction of the computation effort.

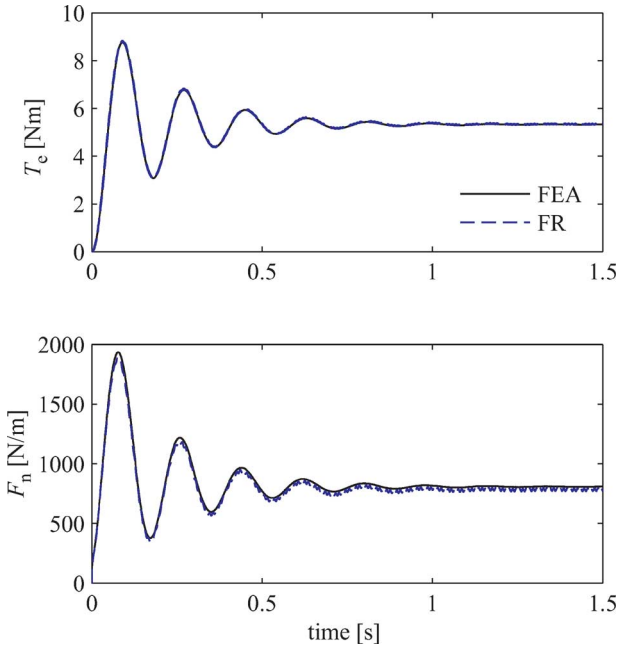


Fig. 11. Comparison of torque and radial force calculation.

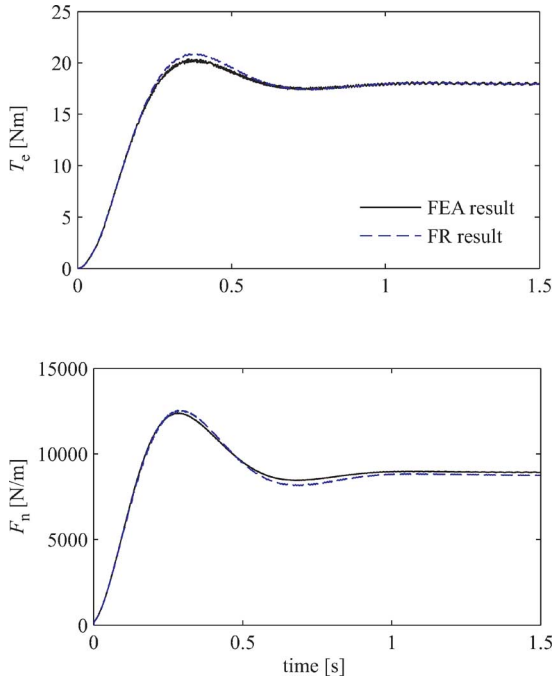


Fig. 12. Torque and radial force responses of field-oriented control startup.

### B. Current-Regulated Field-Oriented Control

Proven to have wide bandwidth dynamic performance, the indirect field-oriented control is commonly used in high-performance induction motor drives. An indirect field-oriented control method is implemented in the FEA and FR programs as [18]

$$\frac{d\theta_e}{dt} = \omega_e = \frac{P}{2}\omega_{\rm rm} + \frac{i^e_{\rm qs}}{\tau_r i^e_{\rm ds}} \tag{26}$$

$$\begin{bmatrix} i_{\rm as} \\ i_{\rm bs} \\ i_{\rm cs} \end{bmatrix} = \begin{bmatrix} \cos\theta_e & \sin\theta_e \\ \cos\left(\theta_e - \frac{2\pi}{3}\right) & \sin\left(\theta_e - \frac{2\pi}{3}\right) \\ \cos\left(\theta_e + \frac{2\pi}{3}\right) & \sin\left(\theta_e + \frac{2\pi}{3}\right) \end{bmatrix} \begin{bmatrix} i^e_{\rm qs} \\ i^e_{\rm ds} \end{bmatrix} \tag{27}$$

where $i^e_{\rm qs}$ and $i^e_{\rm ds}$ are the $q$- and $d$-axis stator currents and $\tau_r$ is the rotor electrical time constant. The value of rotor time constant is 0.21 s, which was obtained from the FEA model using the characterization method suggested in [19]. By keeping $i^e_{\rm ds}$ constant, the field-oriented control is achieved. It is assumed that the motor is initially deenergized and the initial motor speed is zero. The load torque is assumed to be proportional to the square of the rotor speed with rated torque produced at rated speed. The moment of inertia of the rotor is $J = 0.03\ {\rm kg}\cdot{\rm m}^2$. After $t = 0$, $i^e_{\rm ds} = 10.1$ A, and $i^e_{\rm qs} = 17.8$ A. The step sizes for both methods are 0.001 s. The simulation ends at $t = 1.5$ s. For this study, the FEA program required about 220 min to complete the simulation, while FR program requires 3 min. The startup simulation results, which include electromagnetic torque, radial force, and motor speed, are shown in Figs. 12 and 13, respectively. In the figures, the solid lines are for the FEA result and the dashed lines are for the FR result. Using the result of the FEA method as a reference, the torque estimation error by the FR method is less than 3%, and it decays to zero in steady state. The speed estimation error is less than 2% and it converges to zero in steady state.

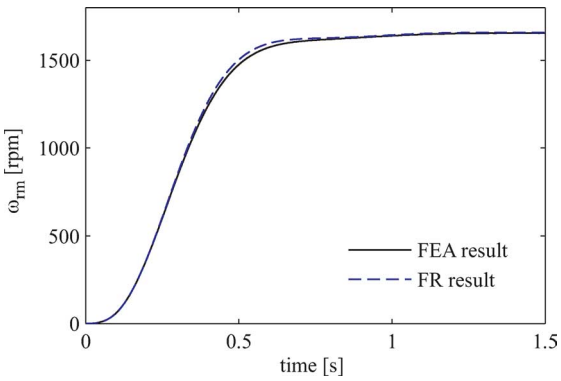


Fig. 13. Field-oriented control startup speed response.

## VI. Discussions

The FR-based modeling approach represents an alternative to using FEA to evaluate machine performance (vector flux densities, torque, and radial force) under arbitrary stator current input. It is recognized that a classic method of characterizing machine performance is to use a *qd* model. Specifically, one can use FEA calculations to obtain the machine response, and then, characterize the machine using an equivalent *qd* circuit.

There are several differences of note between the *qd* and FR models. First, the *qd* model is based on scalar quantities (i.e., only tangential force is calculated). Moreover, the resulting *qd* model does not provide localized values of flux or force

density. Backcalculating the flux densities in the stator/rotor teeth is a nontrivial task. Although the FR only calculates the flux densities in the air gap, these results can be used to approximate stator and rotor tooth flux densities, and thus, also back-iron flux densities quite easily. In addition, obtaining the *q–d* parameters requires several transient FEA evaluations, and then, a characterization routine to fit the model to "measured" data. In the FR technique, which uses the time-domain convolution, the FEA evaluation and the characterization is one in the same.

Finally, in terms of accuracy, several have noted the deficiency of the traditional *qd* model to accurately capture machine performance over a wide range of operating conditions. The inaccuracy is primarily due to the fact that the rotor circuit dynamics are frequency-dependent (i.e., the rotor resistance is frequency-dependent due to skin effect). Several authors have proposed enhanced *qd* models to account the frequency-dependent dynamics [20]–[22]. However, these models require additional FEA evaluations in order to accurately characterize the system. In FR technique, the rotor basis functions are expressed as impulse responses, so the frequency-dependent characteristic is automatically incorporated.

As an example to illustrate the difference in accuracy, the torque versus speed characteristic of the machine used in this research was calculated using a traditional *qd* model and the FR method and the FEA model. The *qd* model was characterized using a parametric fit approach, where steady-state torque data around the rated speed are fitted in a genetic algorithm program [23].

The steady-state torque–speed characteristics of the *qd*, FR models, and the FEA model are shown in Fig. 14, in which the rated voltage is applied. Since the input of the FR technique is stator current, the current values obtained from the FEA solution are used as the input to the FR model. It is observed that the FR technique performs well over the entire speed range. The standard *qd* model yields accurate results in the region where it is characterized. However, the torque prediction error becomes large at low speeds because of the large slip frequency. In today's applications where power electronics are involved, one may argue that such a torque versus speed curve is not relevant, since stator excitation is adjusted to always keep the slip frequency low. However, if the machine is connected to an inverter, where high-frequency switching is introduced, a similar frequency-dependence exists and leads to even larger error in the torque predicted by the traditional *qd* model [20].

As mentioned in Section III, it is assumed that the machine is operated in the linear magnet region. To investigate influence of the magnetic saturation to the FR technique, several additional studies were performed. Under these studies, all the constant-speed described in Section V were repeated with the stator current increased to 40, 60, and 80 A, respectively. With the FEA results as the references, the maximum torque errors are shown in Table II. In addition, the flux density magnitude in the stator teeth and rotor teeth obtained from the FEA program are shown in the table. As expected, it is observed that the performance of the FR model degrades as one operates further into saturation.

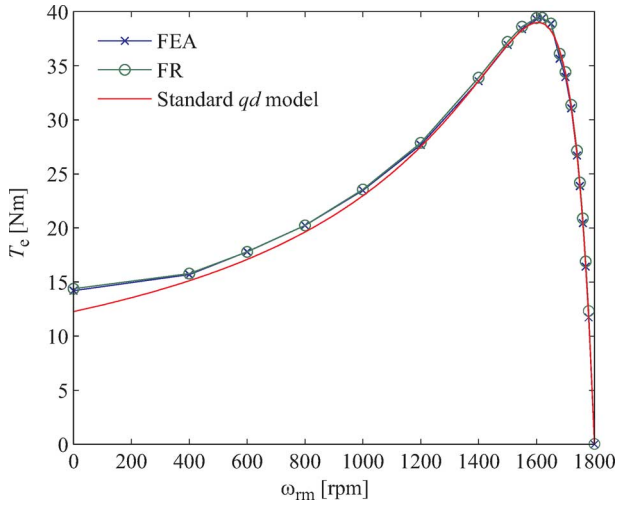


Fig. 14. Torque–speed characteristics of the FEA model, FR model, and standard *qd* model.

TABLE II
TORQUE ERROR OF THE FR TECHNIQUE VERSUS MAGNETIC LOADING

| Stator current amplitude [A] | Maximum torque error | Maximum flux density in rotor teeth [T] | Maximum flux density in stator teeth [T] |
|---|---|---|---|
| 40 | 0.96 % | 1.05 | 1.16 |
| 60 | 8% | 1.5 | 1.53 |
| 80 | 21.9 % | 1.78 | 1.84 |

Finally, it is noted that the basis functions used in FR have some dependence on the rotor position due to the difference in material properties of the rotor bars and teeth. In this paper, the position dependence was neglected and independent basis functions $[k_{\rm ns}(\phi_{\rm sm}), k_{\rm ts}(\phi_{\rm sm}), k_{\rm nr}(\phi_{\rm rm})$, and $k_{\rm tr}(\phi_{\rm rm})]$ were employed. In doing so, one loses the ability to accurately calculate torque ripple due to slot–slot interaction. However, the basis function identification and convolution have been applied to time-varying systems [24]. Therefore, in order to achieve further accuracy of the result and include the slot harmonics effect in the electromagnetic torque, one could characterize a family of basis functions at distinct rotor positions and use a time-varying discrete-time convolution to estimate fields and forces within the machine. This is the topic of ongoing research.

## VII. CONCLUSION

In this paper, a field reconstruction method is proposed for induction machine simulation. The stator and rotor basis functions are identified and stored based upon results of a few FE evaluations. Once basis functions are established, the normal and tangential components of the flux density in the air gap and associated normal and tangential forces are reconstructed under arbitrary stator excitation. The FR results are almost identical to those obtained by the FE method at a fraction of the computational effort.

Although in this paper only a current-source drive is provided, the proposed FR model can be coupled with external circuits. Therefore, the FR technique can be extended to a voltage control

application. It can also be connected to power electronics circuits to evaluate the system level performance of the induction motor drive.

In the simulation results shown in the previous section, three-phase balanced current sources are used as the input. From (19) and (20), it can be seen that the influence of each phase to the flux density in the air gap is independent. Therefore, the FR method is also applicable to the case where the current or voltage source is unbalanced without losing accuracy.

## REFERENCES


[1] F. Blaschke, "The principle of field orientation as applied to the new transvector closed-loop control system for rotating-field machines," *Siemens Rev.*, vol. 39, no. 5, pp. 217–220, 1972.

[2] H. A. Toliyat, E. Levi, and M. Raina, "A review of RFO induction motor parameter estimation techniques," *IEEE Trans. Energy Convers.*, vol. 18, no. 2, pp. 271–283, Jun. 2003.

[3] D. W. Novotny and T. A. Lipo, *Vector Control and Dynamics of AC Drives*. London, U.K.: Oxford Univ. Press, 1996.

[4] J. Holtz, "Sensorless control of induction motor drives," *Proc. IEEE*, vol. 90, no. 8, pp. 1358–1394, Aug. 2002.

[5] O. Wasynczuk, S. D. Sudhoff, K. A. Corzine, J. L. Tichenor, P. C. Krause, I. G. Hansen, and L. M. Taylor, "A maximum torque per ampere control strategy for induction motor drives," *IEEE Trans. Energy Convers.*, vol. 13, no. 2, pp. 163–169, Jun. 1998.

[6] C. Kwon and S. D. Sudhoff, "Genetic algorithm-based induction machine characterization procedure with application to maximum torque per amp control," *IEEE Trans. Energy Convers.*, vol. 21, no. 2, pp. 405–415, Jun. 2006.

[7] M. Bodson, J. N. Chiasson, and R. T. Nototnak, "A systematic approach to selecting flux references for torque maximization in induction motors," *IEEE Trans. Control Syst. Technol.*, vol. 3, no. 4, pp. 387–397, Dec. 1995.

[8] I. Takahashi and Y. Ohmori, "High-performance direct torque control of an induction motor," *IEEE Trans. Ind. Appl.*, vol. 25, no. 2, pp. 257–264, Mar./Apr. 1989.

[9] T. G. Habetler, F. Profumo, M. Pastorelli, and L. M. Tolbert, "Direct torque control of induction machines using space vector modulation," *IEEE Trans. Ind. Appl.*, vol. 28, no. 5, pp. 1045–1053, Sep./Oct. 1992.

[10] J.-K. Kang and S.-K. Sul, "New direct torque control of induction motor for minimum torque ripple and constant switching frequency," *IEEE Trans. Ind. Appl.*, vol. 35, no. 5, pp. 1076–1082, Sep./Oct. 1999.

[11] A. Tripathi, A. M. Khambadkone, and S. K. Panda, "Space-vector based, constant frequency, direct torque control and dead beat stator flux control of AC machines," in *Proc. Int. Conf. Ind. Electron. (IECON'01)*, vol. 2, pp. 1219–1224.

[12] P. Z. Grabowski, M. P. Kazmierkowski, B. K. Bose, and F. Blaabjerg, "A simple direct-torque neuro-fuzzy control of PWM-inverter-Fed induction motor drive," *IEEE Trans. Ind. Electron.*, vol. 47, no. 4, pp. 863–870, Aug. 2000.

[13] W. Zhu, B. Fahimi, and S. D. Pekarek, "A field reconstruction method for optimal excitation of permanent magnet synchronous machines," *IEEE Trans. Energy Convers.*, vol. 21, no. 2, pp. 305–313, Jun. 2006.

[14] S. J. Salon, *Finite Element Analysis of Electrical Machines*. Norwell, MA: Kluwer, 1995.

[15] L. Chang, A. R. Eastham, and G. E. Dawson, "Permanent magnet synchronous motors: finite element torque calculations," in *Proc. IEEE IAS Annu. Meet. 1989*, vol. 1, pp. 69–73, Oct. 1989.

[16] A. V. Oppenheim, A. S. Willsky, and S. H. Nawab, *Signals and Systems*, 2nd ed. Upper Saddle River, NJ, Prentice-Hall, 1997.

[17] *Maxwell 2D Field Simulator Manuals,* Ansoft Corp., Pittsburgh, PA, 2002.

[18] P. C. Krause, O. Wasynczuk, and S. D. Sudhoff, *Analysis of Electric Machinery and Drive Systems*. Piscataway, NJ: IEEE Press, 2002.

[19] J. Joddar, W. Zhu, B. Fahimi, and S. D. Pekarek, "An investigation into the electromagnetic behavior of the vector controlled induction motor drives," in *Proc. IEEE IAS Annu. Meet. 2004*, Rolla, MO, vol. 1, pp. 17, Oct.

[20] S. D. Sudhoff, D. C. Aliprantis, B. T. Kuhn, and P. L. Chapman, "An induction machine model for predicting inverter-machine interaction," *IEEE Trans. Energy Convers.*, vol. 17, no. 2, pp. 203–210, Jun. 2002.

[21] W. Levy, C. F. Landy, and M. D. McCulloch, "Improved models for the simulation of deep bar induction motors," *IEEE Trans. Energy Convers.*, vol. 5, no. 2, pp. 393–400, Jun. 1990.

[22] N. Retiere, A. Foggia, D. Roye, and P. Mannevy, "Deep-bar induction motor model for large transient analysis under saturated conditions," in *IEEE Int. Electr. Mach. Drives Conf. Rec.*, May 1997, pp. MD1/3.1–MD1/3.3.

[23] "Genetic Optimization System Engineering Tool (GOSET) for use with MATLAB/Manual Version 2.2," School Electr. Comput. Eng., Purdue Univ., West Lafayette, IN, with United States Naval Academy, Annapolis, MD, 2005.

[24] C.-T. Chen, *Linear System Theory and Design*, 3rd ed. London, U.K.: Oxford Univ. Press, 1999.


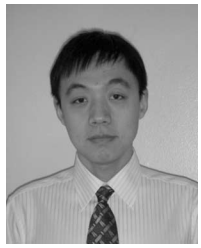

**Dezheng Wu** received the B.Eng. degree from Shanghai Jiao Tong University, Shanghai, China, in 2000, and the M.Eng. degree from the National University of Singapore, Singapore, in 2005, both in electrical engineering. He is currently working toward the Ph.D. degree in electrical engineering at Purdue University, West Lafayette, IN.

His current research interests include design, analysis, and control of electric machines.

**Steve Pekarek** (M'97) received the Ph.D. degree in electrical engineering from Purdue University, West Lafayette, IN, in 1996.

From 1997 to 2004, he was an Assistant (Associate) Professor of electrical and computer engineering at the University of Missouri–Rolla (UMR). He is currently a Professor of electrical and computer engineering at Purdue University, where he is also the Chair of the Energy Sources and Systems Area.He has been the Principal Investigator on a number of successful research programs including projects for the Navy, Air Force, Ford Motor Company, Motorola, and Delphi Automotive Systems. The primary focus of these investigations has been the analysis and design of power electronic-based architectures for finite inertia power and propulsion systems.

Prof. Pekarek is the Chair of the 2008 IEEE Applied Power Electronics Conference. He is a member of the IEEE Power Engineering Society, the Society of Automotive Engineers, and the IEEE Power Electronics Society. He is the recipient of six outstanding teaching commendations and four faculty excellence awards from the UMR.

**Babak Fahimi** (S'96–M'99–SM'02) received the Ph.D. degree in electrical engineering from Texas A&M University, College Station, in 1999.

During 1999–2002, he was a Research Scientist at Electrostandards Laboratories, Inc., Cranston, RI. During 2002–2004, he was an Assistant Professor in the Department of Electrical and Computer Engineering, University of Missouri-Rolla. He is currently with the Department of Electrical Engineering, University of Texas, Arlington. He is the author or coauthor of more than 80 technical papers and several book chapters including a chapter in John Wiley Encyclopedia on electrical and electronics engineering. He is the holder of two U.S. patents and has several pending patents.

Dr. Fahimi is the Editor for the IEEE TRANSACTIONS ON ENERGY CONVERSION, an Associate Editor for the IEEE TRANSACTIONS ON POWER ELECTRONICS, and the Technical Program Chair for the International Conference on Electric Machinery and Drives, 2005, San Antonio, TX. He is a member of the Society of Automotive Engineers (SAE). He was the recipient of the Richard M. Bass Young Power Electronics Investigator Award from the IEEE Power Electronics Society in 2003, the Office of Naval Research Young Investigator Award in 2004, and the German Academic Exchange International Fellowship in 1993–1995.